Hindawi Publishing Corporation
International Journal of Engineering Mathematics
Volume 2015, Article ID 287623, 15 pages
http://dx.doi.org/10.1155/2015/287623

Research Article

Mixed Convection Flow of Magnetic Viscoelastic Polymer from a Nonisothermal Wedge with Biot Number Effects

S. Abdul Gaffar,[1] V. Ramachandra Prasad,[2] Bhuvana Vijaya,[1] and O. Anwar Beg[3]

[1]*Department of Mathematics, Jawaharlal Nehru Technological University Anantapur, Anantapur 515002, India*
[2]*Department of Mathematics, Madanapalle Institute of Technology and Science, Madanapalle 517325, India*
[3]*Gort Engovation Research (Aerospace and Medical Engineering), 11 Rooley Corft, Bradford BD6 1FA, UK*

Correspondence should be addressed to S. Abdul Gaffar; abdulsgaffar0905@gmail.com

Received 4 May 2015; Revised 5 September 2015; Accepted 6 September 2015

Academic Editor: Josè A. Tenereiro Machado

Magnetic polymers are finding increasing applications in diverse fields of chemical and mechanical engineering. In this paper, we investigate the nonlinear steady boundary layer flow and heat transfer of such fluids from a nonisothermal wedge. The incompressible Eyring-Powell non-Newtonian fluid model is employed and a magnetohydrodynamic body force is included in the simulation. The transformed conservation equations are solved numerically subject to physically appropriate boundary conditions using a second-order accurate implicit finite difference Keller Box technique. The numerical code is validated with previous studies. The influence of a number of emerging nondimensional parameters, namely, the Eyring-Powell rheological fluid parameter (ε), local non-Newtonian parameter based on length scale (δ), Prandtl number (Pr), Biot number (γ), pressure gradient parameter (m), magnetic parameter (M), mixed convection parameter (λ), and dimensionless tangential coordinate (ξ), on velocity and temperature evolution in the boundary layer regime is examined in detail. Furthermore, the effects of these parameters on surface heat transfer rate and local skin friction are also investigated.

1. Introduction

The development of modern functional materials which can be manipulated using electromagnetic fields has stimulated great attention in polymer engineering sciences in recent years. These materials include ferromagnetic polymers [1], magnetotropic fluids [2], and liquid crystalline electrically conducting polymers [3]. Such fluids exhibit many complex characteristics including non-Newtonian behavior. For better understanding of the manufacture of such materials, *magnetorheological fluid mechanics* plays a central role. Although many different magnetic properties may arise in such materials, a fundamental methodology for their synthesis involves the application of transverse magnetic fields which alters momentum transfer and therefore also influences coupled processes such as heat transfer and mass transfer (species diffusion). Many constitutive material models have been developed to simulate the departure of such fluids from Newtonian viscous behavior. In these fluids, the constitutive relationship between stress and rate of strain is nonlinear in comparison to the Navier-Stokes equations which are generally good for Newtonian fluids. Most non-Newtonian models involve some form of modification to the momentum conservation equations. A comprehensive summary of such models which include the Maxwell model, power-law model, and also Eyring-Powell and Giesekus viscoelastic models, is provided in the treatise by Shaw [4]. Heat transfer is often also frequently present in polymer dynamics [5]. Furthermore, in many polymer fabrication flows, *boundary layer phenomena* arise. The *convective boundary condition* has therefore also attracted some interest and this is usually simulated via a Biot number in the wall thermal boundary condition. Recently, Ishak [6] discussed the similarity solutions for flow and heat transfer over a permeable surface with convective boundary condition. Aziz [7] provided a similarity solution for laminar thermal boundary layer over a flat surface with a convective surface boundary condition. Aziz [8] further studied hydrodynamic and thermal slip flow boundary layers with an isoflux thermal boundary condition. Buoyancy effects

on thermal boundary layers subject to a convective surface boundary condition were examined by Makinde and Olanrewaju [9]. Gupta et al. [10] used a variational finite element to simulate mixed convective-radiative non-Newtonian shrinking sheet flow with a convective boundary condition and Eringen's micropolar material model. Swapna et al. [11] studied convective wall heating effects on hydromagnetic flow of a micropolar fluid. Makinde et al. [12] studied cross diffusion effects and Biot number influence on hydromagnetic Newtonian boundary layer flow with homogenous chemical reactions and MAPLE quadrature routines. Bég et al. [13] analyzed Biot number and buoyancy effects on magnetohydrodynamic thermal slip flows. Subhashini et al. [14] studied wall transpiration and cross diffusion effects on free convection boundary layers with a convective boundary condition. In many of these studies, magnetohydrodynamic effects were also considered generally via the introduction of a Lorentzian magnetic drag force and consideration of the Hartmann number. Relatively few studies however have considered magnetic field effects on *Eyring-Powell* viscoelastic polymer flows. This rheological model has certain advantages over the other non-Newtonian formulations, including simplicity, ease of computation, and physical robustness. Furthermore, it is deduced from kinetic theory of liquids rather than the empirical relation. Additionally, it correctly reduces to Newtonian behavior for low and high shear rates [15]. It is a three-constant model which displays a nonzero bounded viscosity at both the upper and the lower limits. Distinct from the popular Ostwald-De Waele power-law model, the Eyring-Powell model does not demonstrate infinite effective viscosities for low shear rates. Investigations employing this model of relevance to polymeric transport processes include Hayat et al. [16] in radiative magnetic convection, Sirohi et al. [17] for wedge flows, and Adesanya and Gbadeyan [18] for channel flows. Very recently, Prasad et al. [19] studied the thermal convection flow in permeable materials with Biot number effects, observing that increasing rheological effect accelerates the flow and heats the boundary layer.

Very few of the above studies have considered *Falkner-Skan flows* [20]. This family of boundary layer flows is associated with the two-dimensional wedge configuration. Non-Newtonian flows from wedge bodies arise in a number of chemical engineering systems which have been described in detail by Peddieson [21] employing the second-order Reiner-Rivlin model. The mixed convection boundary layer flow from a heated wedge plate has also drawn some interest. The combined forced and free convection flow and heat transfer about a nonisothermal wedge subject to a nonuniform free stream velocity were first considered by Sparrow et al. [22]. Watanabe et al. [23] analyzed theoretically mixed convection flow over a perforated wedge with uniform suction or injection. Kafoussias and Nanousis [24] and Nanousis [25] studied the effect of suction or injection on MHD mixed convection flow past a wedge. Gorla [26] used a power-law model to study heat transfer in polymer flow past a wedge. Yih [27] evaluated radiation effects on mixed convection flow about an isothermal wedge embedded in a saturated porous medium. Rashidi et al. [28] developed homotopy solutions for third grade viscoelastic flow from a nonisothermal wedge. Chamkha et al. [29] presented computational solutions for MHD forced convection flow from a nonisothermal wedge in the presence of a heat source or sink with a finite difference method. Hsiao [30] reported on MHD convection of viscoelastic fluid past a porous wedge, observing that the elastic effect increases the local heat transfer coefficient and heat transfer rates at the wedge surface. Ishak et al. [31] obtained a self-similar solution for a moving wedge in a micropolar fluid. Ishak et al. [32] further studied numerically steady two-dimensional laminar flow past a moving wedge in non-Newtonian fluid.

The objective of the present study is to investigate the laminar boundary layer flow and heat transfer of an *Eyring-Powell* non-Newtonian fluid from a nonisothermal wedge. Such a study has not appeared in the literature to the knowledge of the authors. The nondimensional equations with associated dimensionless boundary conditions are solved with the Keller implicit finite difference "Box" scheme [33]. The effects of the emerging thermophysical parameters, namely, *the rheological parameters* (ε, δ), *Biot number* (γ), *mixed convection parameter* (λ), *pressure gradient parameter* (m), *magnetic parameter* (M), *and Prandtl number* (Pr), on the velocity, temperature, local skin friction, and heat transfer rate (local Nusselt number) characteristics are studied. The present problem is relevant to the simulation of magnetized polymer materials fabrication processes.

2. Non-Newtonian Constitutive Eyring-Powell Fluid Model

In the present study, a subclass of non-Newtonian fluids known as the *Eyring-Powell fluid* is employed. The Cauchy stress tensor for Eyring-Powell fluids [15] takes the hyperbolic form:

$$\tau_{ij} = \mu \frac{\partial u_i}{\partial x_j} + \frac{1}{\beta} \sinh^{-1}\left(\frac{1}{C}\frac{\partial u_i}{\partial x_j}\right), \tag{1}$$

where μ is dynamic viscosity and β and C are the rheological fluid parameters of the Eyring-Powell fluid model. Consider the second-order approximation of the $\sinh^{-1}$ function as follows:

$$\sinh^{-1}\left(\frac{1}{C}\frac{\partial u_i}{\partial x_j}\right) \approx \frac{1}{C}\frac{\partial u_i}{\partial x_j} - \frac{1}{6}\left(\frac{1}{C}\frac{\partial u_i}{\partial x_j}\right)^3, \quad \left|\frac{1}{C}\frac{\partial u_i}{\partial x_j}\right| < 1. \tag{2}$$

When the Eyring-Powell formulation is introduced into the subsequent model, the momentum conservation equation is significantly modified with numerous velocity gradient terms including mixed derivatives. Strong nonlinearity therefore results in necessitating numerical solutions. The resulting boundary value problem is found to be well posed and permits an excellent mechanism for the assessment of rheological characteristics on the flow behaviour.

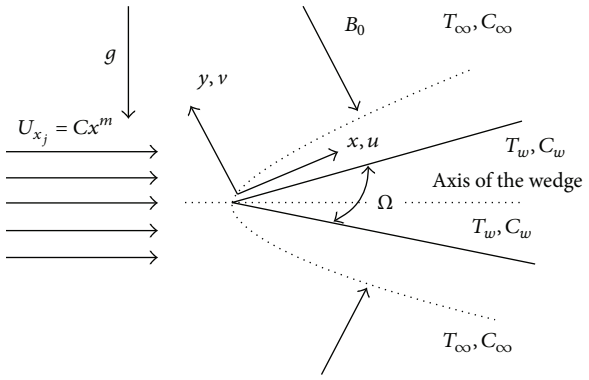

Figure 1: Magnetic polymeric flow from a wedge.

3. Mathematical Thermofluid Polymer Boundary Layer Model

Steady, laminar, and incompressible flow and heat transfer of an Eyring-Powell polymeric fluid from a nonisothermal horizontal wedge are considered, as illustrated in Figure 1.

The x-coordinate (streamwise) is measured along the wall of the wedge and y-coordinate (transverse) is directed normal to it. A uniform magnetic field of strength B_0 is applied parallel to the y-axis, that is, transverse to the wedge surface. Magnetic induction, Hall current, ion slip, and Maxwell displacement currents are neglected. Magnetic Reynolds number is small and the electric field due to polarization of charges is negligible. The gravitational acceleration g acts downwards. We also assume that the Boussinesq approximation holds; that is, density variation is only experienced in the buoyancy term in the momentum equation. Initially, both the wedge and Eyring-Powell fluid are maintained at the same temperature. Instantaneously, they are raised to a temperature $T_w > T_\infty$, the ambient temperature of the fluid which remains unchanged. In line with the approach of Yih [27] and introducing the boundary layer approximations, the equations for *mass, momentum, and energy conservation* can be written as follows:

$$\frac{\partial u}{\partial x} + \frac{\partial v}{\partial y} = 0, \tag{3}$$

$$u\frac{\partial u}{\partial x} + v\frac{\partial u}{\partial y} = U_\infty \frac{dU_\infty}{dx} + \left(\nu + \frac{1}{\rho\beta C}\right)\frac{\partial^2 u}{\partial y^2} - \frac{1}{2\rho\beta C^3}\left(\frac{\partial u}{\partial y}\right)^2 \frac{\partial^2 u}{\partial y^2} \pm g\beta_1 \sin\left(\frac{\Omega}{2}\right)(T - T_\infty), \tag{4}$$

$$u\frac{\partial T}{\partial x} + v\frac{\partial T}{\partial y} = \alpha\frac{\partial^2 T}{\partial y^2}. \tag{5}$$

Here, u and v are the velocity components in x- and y-directions, respectively, $\nu = \mu/\rho$ is the kinematic viscosity of Eyring-Powell fluid (polymer), β_1 is the coefficient of thermal expansion, α is the thermal diffusivity, T is the temperature, and ρ is the density of the fluid. The Eyring-Powell fluid model therefore introduces a *mixed* derivative (second order, second degree) into the momentum boundary layer equation (4). The non-Newtonian effects feature in the shear terms only of (4) and not the convective (acceleration) terms. The fourth term on the right hand side of (4) represents the *thermal buoyancy force* on the flow field, with "+" and "−" signs referring to the *buoyancy-assisting* and *buoyancy-opposing* flow scenarios, and couples the velocity field (4) with the temperature field equation (5). The physical boundary conditions are given as follows:

$$\begin{aligned} &\text{At } y = 0,\\ &\quad u = 0,\\ &\quad v = 0,\\ &-k\frac{\partial T}{\partial y} = h_w\left(T_w - T\right).\\ &\text{As } y \longrightarrow \infty,\\ &\quad u \longrightarrow U_\infty = C_1 x^m,\\ &\quad T \longrightarrow T_\infty. \end{aligned} \tag{6}$$

Here, T_∞ is the free stream temperature, k is the thermal conductivity, h_w is the convective heat transfer coefficient, T_w is the convective fluid temperature, U_∞ is the free stream velocity, and $m = \beta_2/(2-\beta_2)$ is the Hartree pressure gradient parameter which corresponds to $\beta_2 = \Omega/\pi$ for a total angle Ω of the wedge. C_1 is a positive number. The stream function ψ is defined by $u = \partial\psi/\partial y$ and $v = -\partial\psi/\partial x$, and, therefore, the continuity equation is automatically satisfied. In order to render the governing equations and the boundary conditions in dimensionless form, the following nondimensional quantities are introduced:

$$\begin{aligned} \xi &= \frac{\sigma x}{\rho U_\infty},\\ \eta &= \frac{y}{x}\left(\frac{U_\infty x}{\nu}\right)^{1/2},\\ f &= \frac{\psi}{\left(U_\infty x\nu\right)^{1/2}},\\ \theta(\xi,\eta) &= \frac{T - T_\infty}{T_w - T_\infty},\\ \lambda &= \frac{\mathrm{Gr}_x}{\mathrm{Re}_x^2},\\ M &= \frac{\sigma B_0^2 x^2}{\rho\nu\mathrm{Re}_x},\\ \mathrm{Pr} &= \frac{\nu}{\alpha},\\ \mathrm{Gr} &= \frac{g\beta_1\left(T_w - T_\infty\right)x^3}{\nu^2}, \end{aligned}$$

$$\mathrm{Re}_x^2 = \frac{U_\infty x}{\nu},$$
$$\varepsilon = \frac{1}{\mu\beta C},$$
$$\delta = \frac{\nu^2 \mathrm{Re}_x^3}{2C^2 x^4}. \tag{7}$$

All terms are defined in Nomenclature. In view of the transformation defined in (7), the boundary layer equations (4)–(6) are reduced to the following coupled, nonlinear, and dimensionless partial differential equations for momentum and energy for the domain:

$$(1+\varepsilon) f''' + \left(\frac{1+m}{2}\right) ff'' + m\left(1 - f'\right)^2 - \varepsilon\delta \left(f''\right)^2 f''' + \lambda\theta \sin\left(\frac{\Omega}{2}\right) - Mf' = \xi(1-m)\left(f'\frac{\partial f'}{\partial \xi} - f''\frac{\partial f}{\partial \xi}\right), \tag{8}$$

$$\frac{\theta''}{\mathrm{Pr}} + \left(\frac{1+m}{2}\right) f\theta' = \xi(1-m)\left(f'\frac{\partial \theta}{\partial \xi} - \theta'\frac{\partial f}{\partial \xi}\right). \tag{9}$$

The transformed dimensionless boundary conditions are as follows:

$$\begin{aligned} &\text{At } \eta = 0, \\ &f = 0, \\ &f' = 0, \\ &\theta = 1 + \frac{\theta'}{\gamma}. \\ &\text{As } \eta \longrightarrow \infty, \\ &f' \longrightarrow 1, \\ &\theta \longrightarrow 0. \end{aligned} \tag{10}$$

Here, primes denote the differentiation with respect to η and $\gamma = (xh_w/k)\mathrm{Re}_x^{-1/2}$ is the Biot number. The wall thermal boundary condition in (10) corresponds to *convective cooling*. The skin friction coefficient (shear stress at the cylinder surface) and Nusselt number (heat transfer rate) can be defined using the transformations described above with the following expressions:

$$\begin{aligned} \mathrm{Re}_x^{-1/2} C_f &= (1+\varepsilon) f''(\xi, 0) - \frac{\delta}{3}\varepsilon\left(f''(\xi, 0)\right)^3, \\ \mathrm{Re}_x^{-1/2}\mathrm{Nu} &= -\theta'(\xi, 0). \end{aligned} \tag{11}$$

The location, $\xi \sim 0$, corresponds to the vicinity of the *lower stagnation point* on the wedge. For this scenario, the model defined by (8) to (9) contracts to an *ordinary* differential boundary value problem:

$$(1+\varepsilon) f''' + \left(\frac{1+m}{2}\right) ff'' + m\left(1 - f'\right)^2 - \varepsilon\delta \left(f''\right)^2 f''' + \lambda\theta \sin\left(\frac{\Omega}{2}\right) - Mf' = 0, \tag{12}$$
$$\frac{\theta''}{\mathrm{Pr}} + \left(\frac{1+m}{2}\right) f\theta' = 0.$$

The general model is solved using a powerful and unconditionally stable finite difference technique introduced by Keller [33]. The Keller Box method has a second-order accuracy with arbitrary spacing and attractive extrapolation features. It remains one of the most reliable numerical methods for nonlinear boundary layer flows.

4. Numerical Solution with Keller Box Implicit Method

The Keller Box implicit difference method is implemented to solve the nonlinear boundary value problem defined by (8) and (9) with boundary conditions (10). This technique, despite recent developments in other numerical methods, remains a powerful and very accurate approach for boundary layer flow equation systems *which are generally parabolic in nature*. It is unconditionally stable and achieves exceptional accuracy. An excellent summary of this technique is given in Keller [33]. Magnetohydrodynamics applications of Keller's method are reviewed in Anwar Bég [34]. This method has also been applied successfully in many rheological flow problems in recent years. These include oblique micropolar stagnation flows [35], Walter's B viscoelastic flows [36], Stokesian couple stress flows [37], hyperbolic-tangent convection flows from curved bodies [38], micropolar nanofluids [39], Jeffreys elastoviscous boundary layers [40], magnetic Williamson fluids [41], and Maxwell fluids [42]. The Keller Box discretization is *fully coupled* at each step which reflects the physics of parabolic systems, which are also fully coupled. Discrete calculus associated with the Keller Box scheme has also been shown to be fundamentally different from all other mimetic (physics capturing) numerical methods, as elaborated in Anwar Bég [34]. The Keller Box scheme comprises four stages:

(1) Decomposition of the Nth order partial differential equation system to N first-order equations.

(2) Finite Difference Discretization.

(3) Quasilinearization of Nonlinear Keller Algebraic Equations.

(4) Block-tridiagonal elimination solution of the Linearized Keller Algebraic Equations.

The algebraic details for the present problem are provided in Appendix A. A typical mesh is given in Figure 2.

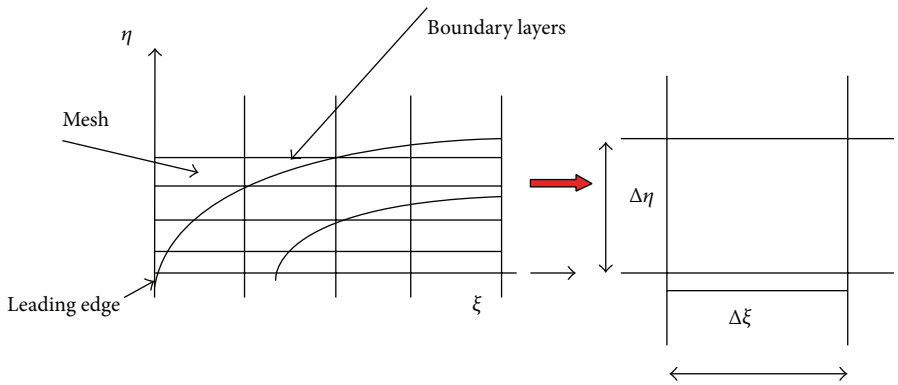

Figure 2: A two-dimensional Keller Box grid.

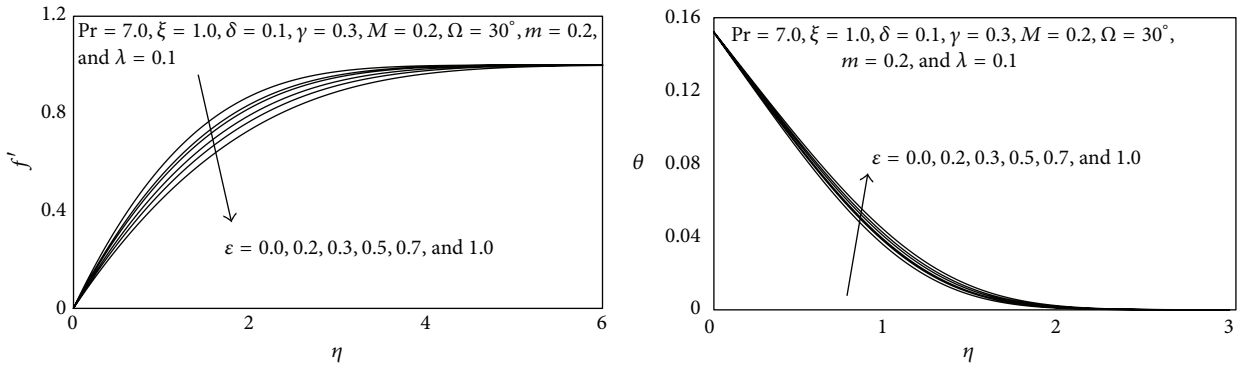

Figure 3: (a) Influence of ε on the Velocity Profiles. (b) Influence of ε on the Temperature Profiles.

5. Numerical Results and Interpretation

Comprehensive solutions have been obtained and are presented in Figures 3–11 and Tables 1–5. The numerical problem comprises two independent variables (ξ, η), two dependent fluid dynamic variables (f, θ), and eight thermophysical and body force control parameters, namely, λ, γ, δ, ε, Pr, ξ, m, and M. The following default parameter values, that is, $\lambda = 0.1$, $\gamma = 0.2$, $\delta = 0.1$, $\varepsilon = 0.1$, Pr = 7.0, $\xi = 1.0$, $m = 0.2$, and $M = 0.2$, are prescribed (unless otherwise stated). Furthermore, the influence of streamwise (transverse) coordinate on heat transfer characteristics is also investigated.

6. Validation with Nakamura Tridiagonal Method (NTM)

To verify the accuracy of the Keller Box method (KBM) code, we have also solved the seventh-order nonlinear partial differential boundary value problem defined by the parabolic equations (8) and (9) with boundary conditions (10), with an alternative finite difference procedure, namely, the Nakamura tridiagonal method (NTM) [43]. NTM is also second order, accurate, and very easily implemented in boundary layer problems. It has proven to be particularly adept at resolving nonlinear and mixed derivatives which characterize non-Newtonian (e.g., viscoelastic) problems. Applications of NTM in rheological boundary layer flows include second-order Reiner-Rivlin wedge convection in porous media [44], power-law convective flows in porous media [45], micropolar wall plume heat transfer [46], and nanofluid bioconvection in permeable materials [47] and magnetohydrodynamic micropolar enrobing flows [48]. Details of the technique with solutions are provided in Appendix B and Tables 6 and 7.

7. Discussion and Interpretation

In Figures 3–11, we note that asymptotically smooth profiles are always achieved in the free stream. An adequate value of infinity has therefore been prescribed in the computations. Figures 3(a) and 3(b) illustrate the effect of Eyring-Powell fluid parameter ε on the velocity (f') and temperature distributions through the boundary layer regime. Velocity is significantly decreased with increasing ε at larger distance from the wedge surface. Conversely, temperature is consistently enhanced with increasing values of ε. The mathematical model reduces to the *Newtonian viscous flow model* as $\varepsilon \to 0$ and $\delta \to 0$. The momentum boundary layer equation in this case contracts to the familiar equation for *Newtonian mixed convection* from a plate; namely, $f''' + ((1+m)/2)ff'' + m(1-(f')^2) + \lambda\theta\sin(\Omega/2) - Mf' = \xi(1-m)(f'(\partial f'/\partial\xi) - f''(\partial f/\partial\xi))$. The thermal boundary layer equation (9) remains unchanged. In Figure 3(b), temperatures are clearly

Table 1: Values of C_f and Nu for different values of Pr, λ, and ε ($\lambda = 0.1$, $\xi = 1.0$, $\delta = 0.1$, $\gamma = 0.3$, $\Omega = 30^\circ$, $m = 0.2$, and $M = 0.2$).

Pr	λ	$\varepsilon = 0.0$		$\varepsilon = 0.2$		$\varepsilon = 0.3$		$\varepsilon = 0.5$		$\varepsilon = 0.7$		$\varepsilon = 1.0$	
		C_f	Nu	C_f	Nu	C_f	Nu	C_f	Nu	C_f	Nu	C_f	Nu
7		0.4867	0.1227	0.5370	0.1201	0.5608	0.1189	0.6065	0.1169	0.6499	0.1151	0.7116	0.1129
10		0.4862	0.1394	0.5365	0.1362	0.5603	0.1349	0.6060	0.1325	0.6494	0.1305	0.7110	0.1278
15		0.4858	0.1608	0.5360	0.1571	0.5598	0.1555	0.6055	0.1527	0.6489	0.1503	0.7104	0.1472
25	0.1	0.4852	0.1924	0.5354	0.1878	0.5593	0.1859	0.6049	0.1824	0.6482	0.1794	0.7098	0.1757
50		0.4846	0.2448	0.5347	0.2389	0.5586	0.2363	0.6042	0.2318	0.6475	0.2279	0.7090	0.2230
75		0.4842	0.2817	0.5344	0.2747	0.5582	0.2717	0.6038	0.2665	0.6471	0.2619	0.7086	0.2562
100		0.4840	0.3111	0.5342	0.3033	0.5580	0.2999	0.6036	0.2941	0.6469	0.2890	0.7084	0.2827
	−0.5	0.4671	0.1219	0.5187	0.1193	0.5422	0.1182	0.5873	0.1162	0.6302	0.1145	0.6912	0.1123
	0.0	0.4817	0.1225	0.5317	0.1199	0.5555	0.1187	0.6011	0.1167	0.6443	0.1149	0.7058	0.1127
	0.5	0.4941	0.1231	0.5447	0.1204	0.5687	0.1192	0.6147	0.1171	0.6583	0.1154	0.7202	0.1131
	1.0	0.5065	0.1237	0.5576	0.1209	0.5819	0.1197	0.6282	0.1176	0.6722	0.1158	0.7346	0.1135
	1.5	0.5188	0.1242	0.5704	0.1215	0.5949	0.1203	0.6417	0.1181	0.6860	0.1163	0.7489	0.1139
	2.0	0.5310	0.1248	0.5831	0.1220	0.6078	0.1208	0.6550	0.1186	0.6997	0.1167	0.7631	0.1143

Table 2: Values of C_f and Nu for different values of λ, δ, and ξ (Pr = 7.0, $\varepsilon = 0.1$, $\gamma = 0.3$, $\Omega = 30^\circ$, $m = 0.2$, and $M = 0.2$).

λ	δ	$\xi = 1.0$		$\xi = 2.0$		$\xi = 3.0$	
		C_f	Nu	C_f	Nu	C_f	Nu
0.2		0.5033	−0.1814	0.4865	−0.1795	0.4793	−0.1787
0.5		0.5148	0.3644	0.4981	0.3608	0.4910	0.3591
1.0	0.1	0.5186	0.5475	0.5010	0.5420	0/4949	0.5395
2.0		0.5205	0.6392	0.5039	0.6329	0.4968	0.6299
3.0		0.5212	0.6697	0.5046	0.6632	0.4974	0.6601
5.0		0.5217	0.6942	0.5051	0.6874	0.4980	0.6842
	0	0.5098	0.1212	0.4931	0.1200	0.4859	0.1194
	3	0.5067	0.1215	0.4903	0.1203	0.4833	0.1197
0.3	5	0.5046	0.1218	0.4884	0.1205	0.4815	0.1200
	7	0.5023	0.1219	0.4865	0.1207	0.4797	0.1202
	8	0.5011	0.1220	0.4855	0.1209	0.4787	0.1203
	10	0.4989	0.1223	0.4836	0.1212	0.4770	0.1206

Table 3: Values of C_f and Nu for different values of m, M, and ξ (Pr = 7.0, $\varepsilon = 0.1$, $\delta = 0.1$, $\lambda = 0.1$, $\gamma = 0.3$, and $\Omega = 30^\circ$).

m	M	$\xi = 1.0$		$\xi = 2.0$		$\xi = 3.0$	
		C_f	Nu	C_f	Nu	C_f	Nu
0.1		0.3237	0.1013	0.3150	0.1008	0.3112	0.1005
0.15		0.4218	0.1121	0.4090	0.1113	0.4036	0.1109
0.2	0.2	0.5097	0.1212	0.4930	0.1200	0.4858	0.1194
0.3		0.6645	0.1363	0.6396	0.1343	0.6291	0.1334
0.4		0.8004	0.1488	0.7672	0.1461	0.7534	0.1450
0.5		0.9247	0.1598	0.8829	0.1565	0.8655	0.1552
	0.0	0.6987	0.1365	0.6824	0.1358	0.6758	0.1354
	0.1	0.4473	0.1151	0.4292	0.1135	0.4215	0.1127
0.2	0.3	0.5924	0.1284	0.5763	0.1275	0.5695	0.1270
	0.4	0.4004	0.1099	0.3809	0.1078	0.3730	0.1070
	0.5	0.3646	0.1054	0.3446	0.1031	0.3365	0.1022

minimized for the Newtonian case ($\varepsilon = 0$) and maximized for the strongest non-Newtonian case ($\varepsilon = 1.0$). The non-Newtonian parameter ε ($= 1/[\mu\beta C]$) is evidently inversely proportional to the viscosity and also to β and C (Eyring-Powell rheological fluid parameters). As ε *is increased, the material viscosity therefore will decrease which would aid momentum development. Similarly, the parameters* β and C *are simultaneously* reduced (they are strongly linked to viscosity) and the overall effect is a boost in material viscosity. This results in reduction in the ε magnitude which manifests in marked deceleration in the flow as shown in Figure 3(a). With decreased momentum diffusion rates, the velocity boundary layer thickness is decreased. Thermal diffusion is conversely enhanced and the fluid is heated (Figure 3(b)), resulting in a thickening in the thermal boundary layer.

Figures 4(a) and 4(b) depict the velocity (f') and temperature (θ) distributions with increasing *local non-Newtonian* parameter, δ. Very little tangible effect is observed in Figure 4(a), although there is a very slight increase in velocity with increase in δ. Similarly, there is only a very slight depression in temperature magnitudes in Figure 4(b) with a rise in δ. This parameter is defined as $\nu^2 \mathrm{Re}_x^3/(2C^2x^4)$ and features in a single negative term in (9), namely, $-\varepsilon\delta(f'')^2 f'''$, unlike the ε rheological parameter which also appears in the shear term, $-(1+\varepsilon)^2 f'''$. This parameter also features viscosity which is effectively decreased weakly and induces a slight acceleration in the flow. The momentum boundary layer thickness is therefore slightly decreased whereas since heat diffusion is decreased, thermal boundary layer thickness is therefore marginally reduced.

Figures 5(a) and 5(b) depict the evolution of velocity (f') and temperature (θ) functions with a variation in Biot number, γ. Dimensionless velocity component (Figure 5(a)) is considerably enhanced with increasing γ. In Figure 5(b), an increase in Biot number is seen to considerably enhance temperatures throughout the boundary layer regime. For $\gamma < 1$, that is, small Biot numbers, the regime is frequently

Table 4: Numerical values of $f''(\xi, 0)$ (in brackets) and skin friction coefficient C_f for different values of δ and ε (Pr = 7.0, $\lambda = 0.1$, $\xi = 1.0$, $\gamma = 0.3$, $\Omega = 30^\circ$, $m = 0.2$, and $M = 0.2$).

$\delta \backslash \varepsilon$	0.0	0.2	0.4	0.6	0.8	1.0
0.0	0.4842	0.5345 (0.4454)	0.5816 (0.4154)	0.6261 (0.3913)	0.6685 (0.3714)	0.7091 (0.3546)
0.1	0.4842	0.5343 (0.4458)	0.5813 (0.4159)	0.6257 (0.3918)	0.6680 (0.3719)	0.7087 (0.3551)
0.2	0.4842	0.5342 (0.4461)	0.5810 (0.4164)	0.6253 (0.3924)	0.6676 (0.3724)	0.7082 (0.3556)
0.3	0.4842	0.5340 (0.4465)	0.5807 (0.4169)	0.6250 (0.3929)	0.6672 (0.3730)	0.7077 (0.3561)
0.4	0.4842	0.5338 (0.4468)	0.5804 (0.4174)	0.6246 (0.3934)	0.6668 (0.3735)	0.7073 (0.3567)
0.5	0.4842	0.5336 (0.4472)	0.5801 (0.4179)	0.6242 (0.3940)	0.6663 (0.3741)	0.7068 (0.3572)
0.6	0.4842	0.5334 (0.4479)	0.5798 (0.4183)	0.6238 (0.3945)	0.6659 (0.3746)	0.7066 (0.3577)
0.7	0.4842	0.5333 (0.4479)	0.5795 (0.4188)	0.6235 (0.3951)	0.6655 (0.3752)	0.7063 (0.3587)
0.8	0.4842	0.5331 (0.4482)	0.5792 (0.4194)	0.6231 (0.3956)	0.6650 (0.3758)	0.7054 (0.3588)
0.9	0.4842	0.5329 (0.4486)	0.5788 (0.4204)	0.6227 (0.3962)	0.6646 (0.3763)	0.7049 (0.3594)
1.0	0.4842	0.5327 (0.4490)	0.5786 (0.4204)	0.6223 (0.3968)	0.6642 (0.3769)	0.7024 (0.3589)

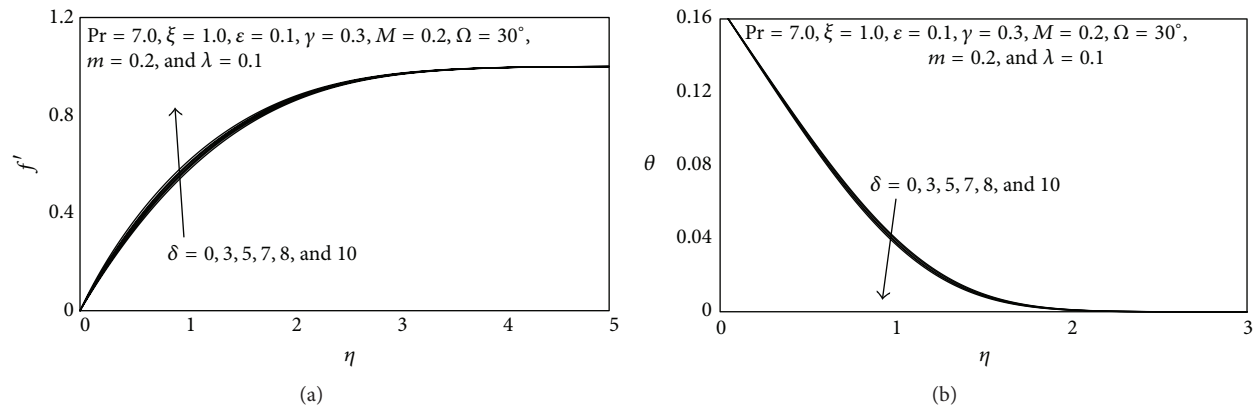

Figure 4: (a) Influence of δ on the Velocity Profiles. (b) Influence of δ on the Temperature Profiles.

Table 5: Comparison values of Nu for different values of λ when $m = 1$, Pr = 0.72, and $\varepsilon = \delta = 0$.

λ	Yacob et al. [49]	Present
0.0	1.1244	1.1243
−0.2	0.9113	0.9112
−0.4	0.6749	0.6747
−0.6	0.4386	0.4388
−0.8	0.1828	0.1829

Table 6: Values of C_f and Nu for different values of m, M, and ξ (Pr = 7.0, $\varepsilon = 0.1$, $\delta = 0.1$, $\lambda = 0.1$, $\gamma = 0.3$, and $\Omega = 30^\circ$).

		$\xi = 1.0$		$\xi = 1.0$	
m	M	C_f KBM	Nu KBM	C_f NTM	Nu NTM
0.1	0.2	0.3237	0.1013	0.3238	0.1011
0.15		0.4218	0.1121	0.4219	0.1120
0.2		0.5097	0.1212	0.5095	0.1210
0.3		0.6645	0.1363	0.6647	0.1365
0.4		0.8004	0.1488	0.8005	0.1489
0.5		0.9247	0.1598	0.9245	0.1599
0.2	0.0	0.6987	0.1365	0.6988	0.1366
	0.1	0.4473	0.1151	0.4476	0.1154
	0.3	0.5924	0.1284	0.5922	0.1281
	0.4	0.4004	0.1099	0.4001	0.1100
	0.5	0.3646	0.1054	0.3643	0.1053

designated as being "thermally simple" and there is a presence of more uniform temperature fields inside the boundary layer and the wedge solid surface. For $\gamma > 1$, thermal fields are anticipated to be nonuniform within the solid body. The Biot number effectively furnishes a mechanism for comparing the *conduction resistance* within a solid body to the *convection resistance* external to that body (offered by the surrounding fluid) for heat transfer. We also note that a Biot number in excess of 0.1, as studied in Figures 5(a) and 5(b), corresponds to a "thermally thick" substance whereas Biot number less than 0.1 implies a "thermally thin" material. Since γ is inversely proportional to thermal conductivity (k), as γ increases, thermal conductivity will be reduced at the cylinder surface and this will lead to a decrease in the rate of heat transfer from the boundary layer to within the cylinder, manifesting in a rise in temperature at the cylinder surface and in the body of the fluid; the maximum effect will

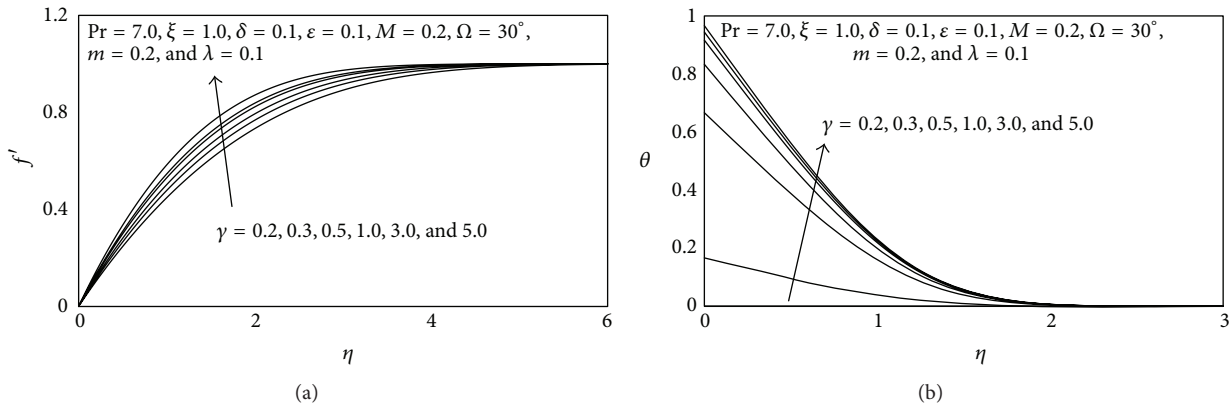

Figure 5: (a) Influence of γ on the Velocity Profiles. (b) Effect of γ on the Temperature Profiles.

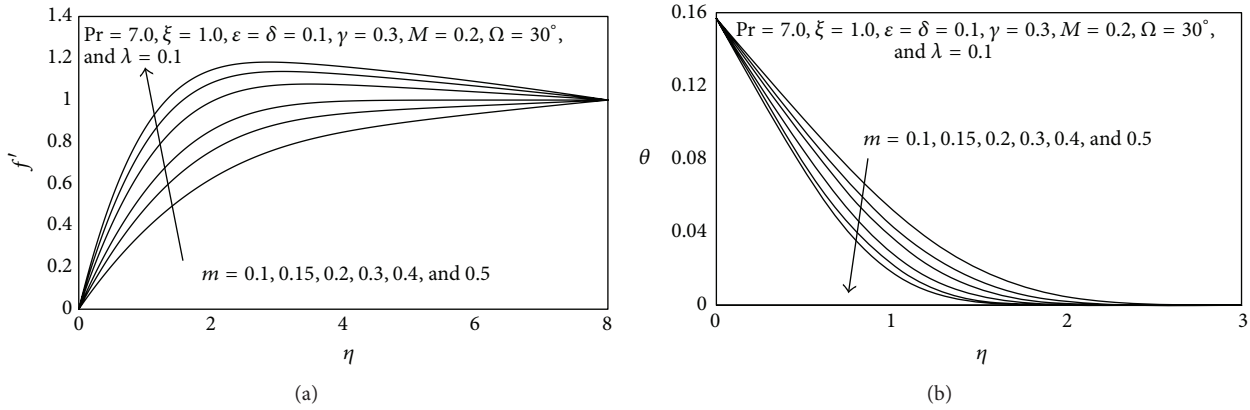

Figure 6: (a) Influence of m on the Velocity Profiles. (b) Influence of m on the Temperature Profiles.

Table 7: Numerical values of skin friction coefficient C_f for different values of δ and ε (Pr = 7.0, $\lambda = 0.1$, $\xi = 1.0$, $\gamma = 0.3$, $\Omega = 30^\circ$, $m = 0.2$, and $M = 0.2$).

$\delta \backslash \varepsilon$	0.0 KBM	0.2 KBM	0.0 NTM	0.2 NTM
0.0	0.4842	0.5345	0.4844	0.5346
0.1	0.4842	0.5343	0.4842	0.5344
0.2	0.4842	0.5342	0.4842	0.5342
0.3	0.4842	0.5340	0.4842	0.5341
0.4	0.4842	0.5338	0.4843	0.5338
0.5	0.4842	0.5336	0.4842	0.5337
0.6	0.4842	0.5334	0.4842	0.5335

be sustained at the surface, as witnessed in Figure 5(b). For a fixed wall convection coefficient and thermal conductivity, Biot number as defined in $\gamma = (xh_w/k)\mathrm{Re}_x^{-1/2}$ is also inversely proportional to the local Reynolds (free convection) number. However, as the Biot number increases, the local Reynolds number must decrease and this will induce the opposite effect, that is, *accelerating the boundary layer flow*, as shown in Figure 5(a).

Figures 6(a) and 6(b) depict the profiles for velocity (f') and temperature (θ) for various values of pressure gradient parameter, m. It is observed that increasing m significantly accelerates the flow; that is, velocity increases. This trend is familiar from other studies, for example, Nanousis [25] and Gorla [26]. However, increasing m is found to decelerate the temperature. Effectively, with greater pressure gradient effect, the momentum boundary layer thickness is reduced and thermal boundary layer thickness is decreased. In (9), with $m = 0$, the wedge flow becomes *Blasius flow from a flat plate*. With $m = 1$, we retrieve the case of flow in the vicinity of *stagnation point flow on an infinite plate*. While these two flow cases are of mathematical interest, in practical polymer processing, they are not. The generalized wedge case is more relevant for which $m \neq 0$, as studied in Figures 6(a) and 6(b).

Figures 7(a) and 7(b) depict the profiles for velocity (f') and temperature (θ) for various values of mixed convection parameter, λ. It is found that an increase in λ increases the velocity. However, the temperature decreases significantly. The mixed convection parameter $\lambda = \mathrm{Gr}_x/\mathrm{Re}_x^2$ couples the momentum field with the energy field, via the buoyancy term, $\lambda\theta\sin(\Omega/2)$. Although this is a first-order term, it has a profound influence on the interplay of velocity and temperature. With positive values, we have *buoyancy-aided* flow and with negative values we have *buoyancy-opposed* flow.

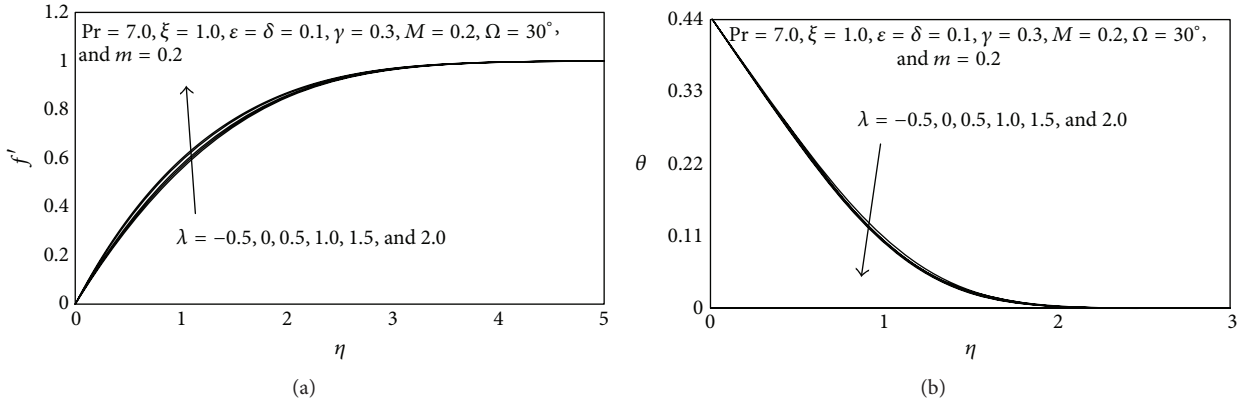

Figure 7: (a) Influence of λ on the Velocity Profiles. (b) Influence of λ on the Temperature Profiles.

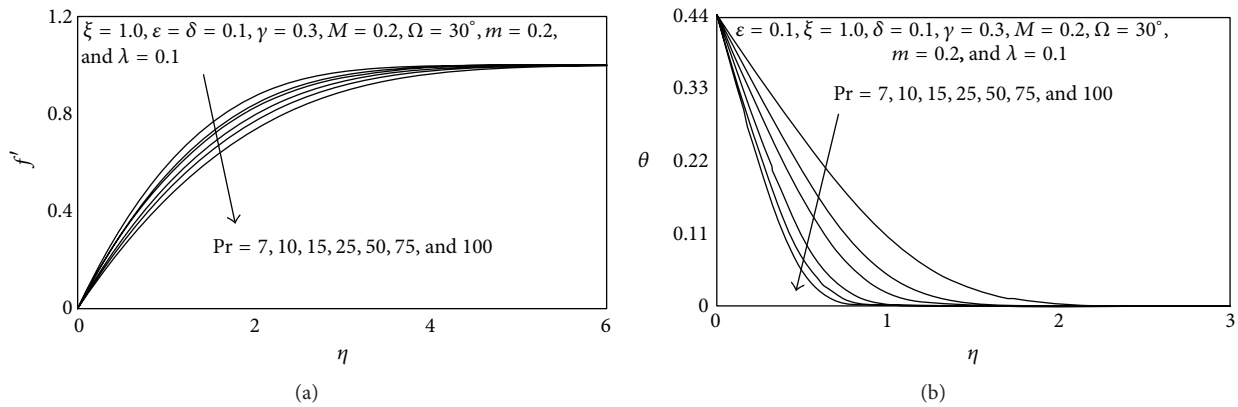

Figure 8: (a) Influence of Pr on the Velocity Profiles. (b) Influence of Pr on the Temperature Profiles.

Both are studied in Figures 7(a) and 7(b). Evidently when buoyancy aids the flow ($\lambda > 0$), velocities are increased, with the contrary effect for buoyancy opposition. The momentum boost achieved with assistive buoyancy force results however in a depletion of thermal energy which cools the boundary layer and decreases temperatures (Figure 7(b)). The reverse effect is generated with opposing buoyancy force which heats the boundary layer and increases thermal boundary layer thickness.

Figures 8(a) and 8(b) depict the profiles for velocity (f') and temperature (θ) for various values of Prandtl number, Pr. It is observed that an increase in the Prandtl number significantly decelerates the flow; that is, velocity decreases. Also increasing Prandtl number is found to decelerate the temperature. Prandtl numbers of 100 are more representative of weak polymer solutions and are associated with slower and cooler flows. Momentum boundary layer thickness is greater for such fluids as is thermal boundary layer thickness.

Figures 9(a) and 9(b) depict the profiles for velocity (f') and temperature (θ) for various values of magnetic parameter, M. It is observed that an increase in M significantly decelerates the flow; that is, velocity decreases. Conversely, increasing M is found to enhance the temperature. The parameter, M, is a Hartmann number. It simulates the relative contribution of Lorentzian magnetohydrodynamic drag force relative to viscous hydrodynamic force. As M is increased, greater opposition is generated to the flow past the wedge leading to deceleration. The supplementary work expended in dragging the polymer against the imposition of the transverse magnetic field creates heating in the polymer. This dissipation of heat leads to a temperature rise and thickening of thermal boundary layers in polymers. Such phenomena are documented extensively in magnetohydrodynamic studies, for example, in Makinde et al. [12] and Chamkha et al. [29].

Figures 10(a) and 10(b) show the influence of Eyring-Powell fluid parameter, ε, on dimensionless skin friction coefficient ($(1+\varepsilon)\xi f''(\xi,0) - (\delta/3)\varepsilon\xi^3(f'''(\xi,0))^3$) and heat transfer rate ($-\theta'(\xi,0)$) at the wedge surface. It is observed that the dimensionless skin friction is increased with the increase in ε; that is, the boundary layer flow is accelerated with decreasing viscosity effects in the non-Newtonian regime. Conversely, the surface heat transfer rate is substantially *decreased* with increasing ε values. Decreasing viscosity of the fluid (induced by increasing the ε value) reduces thermal diffusion as compared with momentum diffusion. A decrease in heat transfer rate at the wall will imply that less heat is convected from the fluid regime to the wedge, thereby heating the boundary layer and enhancing temperatures.

Figures 11(a) and 11(b) illustrate the influence of the local non-Newtonian parameter, δ, on the dimensionless skin

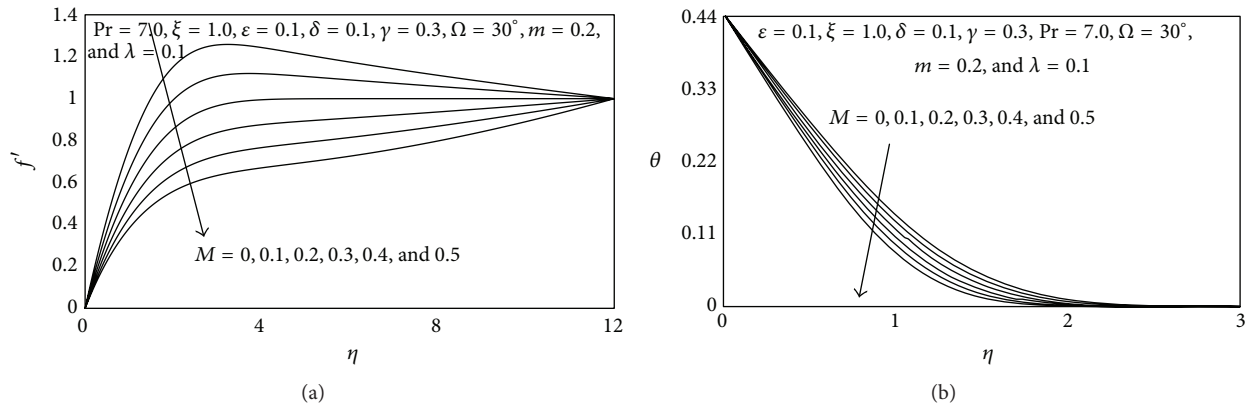

FIGURE 9: (a) Influence of M on the Velocity Profiles. (b) Influence of M on the Temperature Profiles.

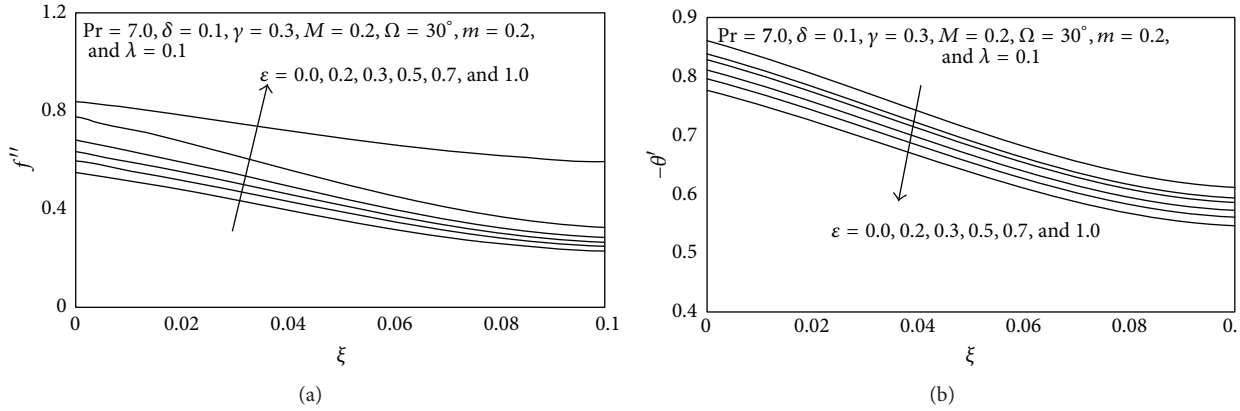

FIGURE 10: (a) Influence of ε on skin friction coefficient. (b) Influence of ε on Nusselt number.

friction coefficient $((1+\varepsilon)\xi f''(\xi,0)-(\delta/3)\varepsilon\xi^3(f'''(\xi,0))^3)$ and heat transfer rate $(-\theta'(\xi,0))$. The skin friction (Figure 11(a)) at the wedge surface is accentuated with increasing δ, however only for very large values of the transverse coordinate, ξ. The flow is therefore strongly accelerated along the wedge surface far from the lower stagnation point. Heat transfer rate (local Nusselt number) is also enhanced with increasing δ, *again at large values of* ξ, as computed in Figure 11(b).

In Table 1, we present the influence of the Eyring-Powell fluid parameter, ε, on the skin friction and heat transfer rate, along with a variation in Pr and λ. With increasing ε, the skin friction is enhanced. The parameter ε is inversely proportional to the dynamic viscosity of the non-Newtonian fluid. There as ε is elevated, viscosity will be reduced and this will induce lower resistance to the flow at the surface of the wedge, that is, accelerating the flow leading to an *escalation* of shear stress. Furthermore, this trend is sustained at any Pr. However, an increase in Pr markedly reduces the shear stress magnitudes. Similarly increasing ε is observed to reduce heat transfer rates, again at all Pr's, whereas Pr strongly accentuates heat transfer rates. Magnitudes of shear stress are always positive indicating that flow reversal (backflow) never arises. It is also observed that increasing mixed convection parameter, λ, increases both skin friction and heat transfer rates.

Table 2 shows results for the influence of *the local non-Newtonian* parameter (based on length scale x), that is, δ and the mixed convection parameter (λ) along with the variation in ξ on skin friction and heat transfer rate. Skin friction is generally decreased with increasing δ. However, heat transfer rate is found to be enhanced with increasing δ. $\delta = \nu^2\mathrm{Re}_x^3/2C^2x^4$ and inspection of this definition shows that the *effectively inverse proportionality* of δ to kinematic viscosity (ν) (with all other parameters being maintained constant) will generate a strong resistance to the flow leading to a deceleration, that is, drop in shear stresses. Conversely, the direct proportionality of δ to *Reynolds number* (Re_x) will imply that *thermal buoyancy* forces are enhanced as δ increases and this will cause a boost in heat transfer by convection from the wedge surface manifesting with the greater heat transfer rates observed in Table 2. This table also shows that, with an increase in λ, the skin friction and heat transfer rate are elevated.

Table 3 presents the results for the influence of *the pressure gradient* parameter (m) and the magnetic parameter (M) along with the variation in ξ on skin friction and heat transfer rate. Skin friction and heat transfer rate are generally decreased with increasing M. Flow deceleration is therefore confirmed with greater transverse magnetic field, associated with the escalation in Lorentzian magnetohydrodynamic

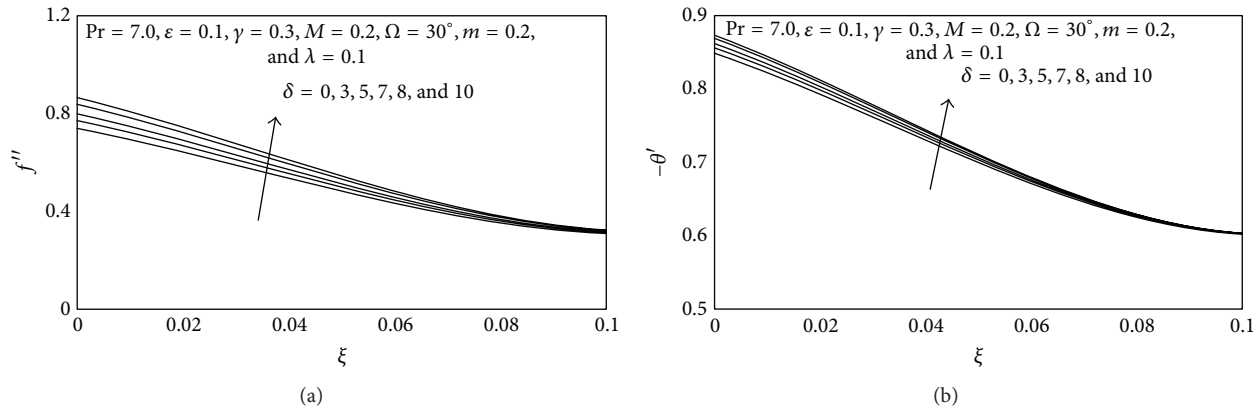

Figure 11: (a) Influence of δ on skin friction coefficient. (b) Influence of δ on Nusselt number.

impedance. However, skin friction and heat transfer rate are found to be enhanced with increasing m.

Table 4 presents the Keller Box numerical solutions of the missing condition $f''(\xi, 0)$ (in brackets) and skin friction C_f for various values of δ and ε. It is found that skin friction is reduced with increasing values of δ. Furthermore, the skin friction C_f is observed to be increased with a rise in the Eyring-Powell fluid parameter (ε) for all values of the *local non-Newtonian* parameter (δ).

Table 5 presents the comparison results of Nu for different values of λ which are found to be in good correlation with those of [49].

8. Conclusions

Numerical solutions have been presented for the nonsimilar, buoyancy-driven boundary layer flow and heat transfer of an Eyring-Powell fluid external to a nonisothermal wedge. This model has been developed to analyse magnetic polymer Falkner-Skan flows of relevance in chemical engineering processing. The Keller Box implicit second-order accurate finite difference numerical scheme has been utilized to efficiently solve the transformed, dimensionless velocity and thermal boundary layer equations, subject to realistic boundary conditions. A comprehensive assessment of the effects of *Eyring-Powell fluid parameter* (ε), *local non-Newtonian parameter* (δ), *Biot number* (γ), *mixed convection parameter* (λ), *pressure gradient parameter* (m), *magnetic body force parameter* (M), and *Prandtl number* (Pr) on thermofluid characteristics has been conducted. Significant flow deceleration has been demonstrated for increasing Eyring-Powell fluid parameter (ε) and negative mixed convection parameter (λ), that is, buoyancy opposition and magnetic body force parameter (M) with generally greater temperatures observed with stronger magnetic field. Excellent correlation with Nakamura tridiagonal method computations has also been achieved, verifying the validity of the present Keller Box solutions. Blasius and stagnation point flow cases have been retrieved as special cases of the generalized wedge flow model. Generally very stable and accurate solutions are obtained with the present finite difference code. The numerical code is able to solve nonlinear boundary layer equations very efficiently and therefore shows excellent promise in simulating transport phenomena in other non-Newtonian fluids. It is therefore presently being employed to study micropolar fluids and viscoplastic fluids which also represent other chemical engineering working fluids. The present study has also neglected time effects. Future simulations will also address *transient* polymeric boundary layer flows and will be presented soon.

Appendices

A. Keller Box Numerical Details

As mentioned earlier, the algebraic details for the Keller Box method are documented here.

Stage 1: Decomposition of Nth-Order Partial Differential Equation System to N First-Order Equations. Equations (8) and (9) subject to the boundary conditions (10) are first cast as a multiple system of first-order differential equations. New dependent variables are introduced:

$$\begin{aligned} u(x, y) &= f', \\ v(x, y) &= f'', \\ s(x, y) &= \theta, \\ t(x, y) &= \theta'. \end{aligned} \tag{A.1}$$

These denote the variables for velocity, temperature, and concentration, respectively. Now, (8) and (9) are solved as a set of fifth-order simultaneous differential equations:

$$f' = u, \tag{A.2}$$

$$u' = v, \tag{A.3}$$

$$\theta' = t, \tag{A.4}$$

$$(1+\varepsilon)\,v' + \left(\frac{1+m}{2}\right) fv + m\left(1-u^2\right) - \varepsilon\delta v^2 v' + \lambda s \sin\left(\frac{\Omega}{2}\right) - Mu = \xi\,(1-m)\left(u\frac{\partial u}{\partial \xi} - v\frac{\partial f}{\partial \xi}\right), \tag{A.5}$$

$$\frac{t'}{\mathrm{Pr}} + \left(\frac{1+m}{2}\right) ft = \xi\,(1-m)\left(u\frac{\partial s}{\partial \xi} - t\frac{\partial f}{\partial \xi}\right), \tag{A.6}$$

where primes denote differentiation with respect to the variable, η. In terms of the dependent variables, the boundary conditions assume the following form:

$$\begin{aligned} &\text{At } \eta = 0,\\ &\quad f = 0,\\ &\quad f' = 0,\\ &\quad \theta = 1 + \frac{\theta'}{\gamma}.\\ &\text{As } \eta \longrightarrow \infty,\\ &\quad f' \longrightarrow 0,\\ &\quad \theta \longrightarrow 0. \end{aligned} \tag{A.7}$$

Stage 2: Finite Difference Discretization. A two-dimensional computational grid is imposed on the ξ-η plane as depicted in Figure 2. The stepping process is defined by

$$\begin{aligned} &\eta_0 = 0,\\ &\eta_j = \eta_{j-1} + h_j, \quad j = 1, 2, \ldots, J,\\ &\eta_J \equiv \eta_\infty,\\ &\xi^0 = 0,\\ &\xi^n = \xi^{n-1} + k_n, \quad n = 1, 2, \ldots, N, \end{aligned} \tag{A.8}$$

where k_n is the $\Delta\xi$-spacing and h_j is the $\Delta\eta$-spacing.

If g_j^n denotes the value of any variable at (η_j, ξ^n), then the variables and derivatives of (A.2)–(A.6) at $(\eta_{j-1/2}, \xi^{n-1/2})$ are replaced by

$$\begin{aligned} g_{j-1/2}^{n-1/2} &= \frac{1}{4}\left(g_j^n + g_{j-1}^n + g_j^{n-1} + g_{j-1}^{n-1}\right),\\ \left(\frac{\partial g}{\partial \eta}\right)_{j-1/2}^{n-1/2} &= \frac{1}{2h_j}\left(g_j^n - g_{j-1}^n + g_j^{n-1} - g_{j-1}^{n-1}\right),\\ \left(\frac{\partial g}{\partial \xi}\right)_{j-1/2}^{n-1/2} &= \frac{1}{2k^n}\left(g_j^n - g_{j-1}^n + g_j^{n-1} - g_{j-1}^{n-1}\right). \end{aligned} \tag{A.9}$$

The finite difference approximation of (A.2)–(A.6) for the midpoint $(\eta_{j-1/2}, \xi^n)$ is as follows:

$$\begin{aligned} &h_j^{-1}\left(f_j^n - f_{j-1}^n\right) = u_{j-1/2}^n,\\ &h_j^{-1}\left(u_j^n - u_{j-1}^n\right) = v_{j-1/2}^n,\\ &h_j^{-1}\left(s_j^n - s_{j-1}^n\right) = t_{j-1/2}^n,\\ &(1+\varepsilon)\left(v_j - v_{j-1}\right) + \left(\frac{1+m}{2} + \alpha\,(1-m)\right)\\ &\quad\cdot \frac{h_j}{4}\left(f_j + f_{j-1}\right)\left(v_j + v_{j-1}\right) + mh_j\\ &\quad - (m + \alpha\,(1-m))\,\frac{h_j}{4}\left(u_j + u_{j-1}\right)^2 + \frac{\lambda h_j}{2}\\ &\quad\cdot \sin\left(\frac{\Omega}{2}\right)\left(s_j + s_{j-1}\right) - \frac{\varepsilon\delta}{4}\left(v_j + v_{j-1}\right)^2\\ &\quad\cdot \left(v_j - v_{j-1}\right) + \frac{\alpha h_j\,(1-m)}{2} v_{j-1}^{n-1}\left(f_j + f_{j-1}\right)\\ &\quad - \frac{\alpha h_j\,(1-m)}{2} f_{j-1}^{n-1}\left(v_j + v_{j-1}\right)\\ &\quad - \frac{Mh_j}{2}\left(u_j + u_{j-1}\right) = \left[R_1\right]_{j-1/2}^{n-1},\\ &\frac{1}{\mathrm{Pr}}\left(t_j - t_{j-1}\right) + \left(\frac{1+m}{2} + \alpha\,(1-m)\right)\\ &\quad\cdot \frac{h_j}{4}\left(f_j + f_{j-1}\right)\left(t_j + t_{j-1}\right)\\ &\quad - \frac{\alpha h_j\,(1-m)}{4}\left(u_j + u_{j-1}\right)\left(s_j + s_{j-1}\right)\\ &\quad + \frac{\alpha h_j\,(1-m)}{2} s_{j-1/2}^{n-1}\left(u_j + u_{j-1}\right) - \frac{\alpha h_j\,(1-m)}{2}\\ &\quad\cdot u_{j-1/2}^{n-1}\left(s_j + s_{j-1}\right) - \frac{\alpha h_j\,(1-m)}{2}\\ &\quad\cdot f_{j-1/2}^{n-1}\left(t_j + t_{j-1}\right) + \frac{\alpha h_j\,(1-m)}{2}\\ &\quad\cdot t_{j-1/2}^{n-1}\left(f_j + f_{j-1}\right) = \left[R_2\right]_{j-1/2}^{n-1}. \end{aligned} \tag{A.10}$$

Here, we have used the abbreviations:

$$\begin{aligned} &\alpha = \frac{\xi^{n-1/2}}{k_n},\\ &\left[R_1\right]_{j-1/2}^{n-1} = -h_j\left[(1+\varepsilon)\left(v'\right)_{j-1/2}^{n-1}\right.\\ &\quad + \left(\frac{1+m}{2} - \alpha\,(1-m)\right) f_{j-1/2}^{n-1} v_{j-1/2}^{n-1} + m\\ &\quad \left. - (m + \alpha\,(1-m))\left(u_{j-1/2}^{n-1}\right)^2 + \lambda \sin\left(\frac{\Omega}{2}\right) s_{j-1/2}^{n-1}\right. \end{aligned}$$

$$
\begin{aligned}
&- \varepsilon\delta \left(v^2\right)_{j-1/2}^{n-1} \left(v'\right)_{j-1/2}^{n-1} \Bigg], \\
[R_2]_{j-1/2}^{n-1} &= -h_j \left[\frac{1}{\mathrm{Pr}} \left(t'\right)_{j-1/2}^{n-1} \right. \\
&+ \left(\frac{1+m}{2} - \alpha(1-m) \right) f_{j-1/2}^{n-1} t_{j-1/2}^{n-1} \\
&\left. + \alpha(1-m)\, u_{j-1/2}^{n-1} s_{j-1/2}^{n-1} \right].
\end{aligned} \tag{A.11}
$$

The boundary conditions are as follows:

$$
\begin{aligned}
f_0^n &= u_0^n = 0, \\
s_0^n &= 1, \\
u_J^n &= 0, \\
v_J^n &= 0, \\
s_J^n &= 0.
\end{aligned} \tag{A.12}
$$

Stage 3: Quasilinearization of Nonlinear Keller Algebraic Equations. Assuming f_j^{n-1}, u_j^{n-1}, v_j^{n-1}, s_j^{n-1}, t_j^{n-1} to be known for $0 \le j \le J$, then (A.10) constitute a system of $5J + 5$ equations for the solution of $5J + 5$ unknowns f_j^n, u_j^n, v_j^n, s_j^n, t_j^n, $j = 0, 1, 2, \ldots, J$. This *nonlinear* system of algebraic equations is *linearized* by means of Newton's method as explained in [33, 34].

Stage 4: Block-Tridiagonal Elimination Solution of Linear Keller Algebraic Equations. The linearized system is solved by the *block-elimination* method, since it possesses a block-tridiagonal structure. The block-tridiagonal structure generated consists of *block matrices*. The complete linearized system is formulated as a *block matrix system*, where each element in the coefficient matrix is a matrix itself, and this system is solved using the efficient Keller Box method. The numerical results are strongly influenced by the number of mesh points in both directions. After some trials in the η-direction (radial coordinate), a larger number of mesh points are selected whereas in the ξ-direction (tangential coordinate) significantly less mesh points are utilized. $\eta_{\max}$ has been set at 12 and this defines an adequately large value at which the prescribed boundary conditions are satisfied. $\xi_{\max}$ is set at 3.0 for this flow domain. Mesh independence is achieved in the present computations. The numerical algorithm is executed in MATLAB on a PC. The method demonstrates excellent stability, convergence, and consistency, as elaborated by Keller [33].

B. Nakamura Tridiagonal Method (NTM) Verification

For two-dimensional partial differential nonsimilar flows, NTM [43–48] executes the computations using both *inner and outer loops* during the iterative process, the former to advance the solution in the η-direction and the latter to advance it in the ξ-direction. The flow domain is discretized using an equispaced finite difference mesh in the (ξ, η)-directions. The partial derivatives for f, θ with respect to ξ, η are evaluated by central difference approximations. A double iteration loop based on the method of successive substitution is employed. The finite difference discretized equations are solved as a *linear* second-order boundary value problem on the ξ, η-domain. The momentum equation (8) is third-order whereas the heat equation (9) is a *second-order* equation, and for (9), only a *direct* substitution is needed. Setting

$$
\begin{aligned}
P &= f', \\
Q &= \theta.
\end{aligned} \tag{B.1}
$$

Equations (8) and (9) assume the following form.

Nakamura momentum equation is as follows:

$$
A_1 P'' + B_1 P' + C_1 P = S_1. \tag{B.2}
$$

Nakamura heat (energy) equation is as follows:

$$
A_2 Q'' + B_2 Q' + C_2 Q = S_2, \tag{B.3}
$$

where $A_{i=1\cdots3}$, $B_{i=1\cdots3}$, and $C_{i=1\cdots3}$ are the *Nakamura matrix coefficients* and $S_{i=1\cdots3}$ are the *Nakamura source terms* containing a mixture of variables and derivatives associated with the variables (omitted for brevity). The Nakamura equations (B.2) and (B.3) are transformed to finite difference equations and these are orchestrated to form a tridiagonal system which is solved iteratively. Computations are performed in seconds on an SGI Octane dual processor machine. Tables 5 and 6 document the comparison of KBM and NTM solutions for the effects of *pressure gradient* (m), *Hartmann parameter* (M), *streamwise coordinate* (ξ), *and Eyring-Powell rheological parameters* (δ, ε). Excellent agreement is achieved. Confidence in the Keller Box solutions is therefore very high.

Nomenclature

B_0: Constant magnetic field intensity
C_f: Skin friction coefficient
C: Rheological fluid parameter
f: Nondimensional stream function
Gr_x: Local Grashof number
g: Acceleration due to gravity
k: Thermal conductivity of fluid
M: Magnetic parameter
m: Pressure gradient parameter
Nu: Local Nusselt number
Pr: Prandtl number
T: Temperature of the fluid
u, v: Nondimensional velocity components along the x- and y-directions, respectively
V: Velocity vector
x: Streamwise coordinate
y: Transverse coordinate.

Greek Symbols

α: Thermal diffusivity
β: Fluid parameter
ϕ: Nondimensional concentration
η: Dimensionless radial coordinate
μ: Dynamic viscosity
ν: Kinematic viscosity
θ: Nondimensional temperature
ρ: Density of non-Newtonian fluid (polymer)
ξ: Dimensionless tangential coordinate
ψ: Dimensionless stream function
Ω: Total angle of the wedge
λ: Mixed convection parameter
ε: Rheological fluid parameter
γ: Biot number.

Subscripts

w: Conditions at the wall (wedge surface)
∞: Free stream conditions.

Conflict of Interests

The authors declare that there is no conflict of interests regarding the publication of this paper.

References

[1] G. Bossis, O. Volkova, S. Lacis, and A. Meunier, "Magnetorheology: fluids, structures and rheology," in *Ferrofluids: Magnetically Controllable Fluids and Their Applications*, S. Odenbach, Ed., vol. 594 of *Lecture Notes in Physics*, pp. 202–230, Springer, Berlin, Germany, 2002.

[2] J. Rodríguez-López, H. C. Shum, L. Elvira, F. M. de Espinosa, and D. A. Weitz, "Fabrication and manipulation of polymeric magnetic particles with magnetorheological fluid," *Journal of Magnetism and Magnetic Materials*, vol. 326, pp. 220–224, 2013.

[3] S.-F. Fu and X.-Z. Wang, "Effects of magnetic field on shear stress of nematic liquid crystalline polymer under simple shear flow," *Journal of Polymer Science B: Polymer Physics*, vol. 48, no. 17, pp. 1919–1926, 2010.

[4] M. T. Shaw, *Introduction to Polymer Rheology*, Wiley, New York, NY, USA, 2012.

[5] S. Sato, K. Oka, and A. Murakami, "Heat transfer behavior of melting polymers in laminar flow field," *Polymer Engineering & Science*, vol. 44, no. 3, pp. 423–432, 2004.

[6] A. Ishak, "Similarity solutions for flow and heat transfer over a permeable surface with convective boundary condition," *Applied Mathematics and Computation*, vol. 217, no. 2, pp. 837–842, 2010.

[7] A. Aziz, "A similarity solution for laminar thermal boundary layer over a flat plate with a convective surface boundary condition," *Communications in Nonlinear Science and Numerical Simulation*, vol. 14, no. 4, pp. 1064–1068, 2009.

[8] A. Aziz, "Hydrodynamic and thermal slip flow boundary layers over a flat plate with constant heat flux boundary condition," *Communications in Nonlinear Science and Numerical Simulation*, vol. 15, no. 3, pp. 573–580, 2010.

[9] O. D. Makinde and P. O. Olanrewaju, "Combined effects of internal heat generation and buoyancy force on boundary layer flow over a vertical plate with a convective surface boundary condition," *Canadian Journal of Chemical Engineering*, vol. 90, no. 5, pp. 1289–1294, 2012.

[10] D. Gupta, L. Kumar, O. Anwar Bég, and B. Singh, "Finite element simulation of mixed convection flow of micropolar fluid over a shrinking sheet with thermal radiation," *Proceedings of the Institution of Mechanical Engineers Part E: Journal of Process Mechanical Engineering*, vol. 228, no. 1, pp. 61–72, 2014.

[11] G. Swapna, L. Kumar, O. Anwar Bég, and B. Singh, "Effect of thermal radiation on the mixed convection flow of a magneto-micropolar fluid past a continuously moving plate with a convective surface boundary condition," *Journal of Engineering Thermophysics*, In press.

[12] O. D. Makinde, K. Zimba, and O. A. Bég, "Numerical study of chemically-reacting hydromagnetic boundary layer flow with Soret/Dufour effects and a convective surface boundary condition," *International Journal of Thermal and Environmental Engineering*, vol. 4, no. 1, pp. 89–98, 2012.

[13] O. A. Bég, M. J. Uddin, M. M. Rashidi, and N. Kavyani, "Double-diffusive radiative magnetic mixed convective slip flow with Biot and Richardson number effects," *Journal of Engineering Thermophysics*, vol. 23, no. 2, pp. 79–97, 2014.

[14] S. V. Subhashini, N. Samuel, and I. Pop, "Double-diffusive convection from a permeable vertical surface under convective boundary condition," *International Communications in Heat and Mass Transfer*, vol. 38, no. 9, pp. 1183–1188, 2011.

[15] R. E. Powell and H. Eyring, "Mechanisms for the relaxation theory of viscosity," *Nature*, vol. 154, no. 3909, pp. 427–428, 1944.

[16] T. Hayat, S. Asad, M. Mustafa, and A. Alsaedi, "Radiation effects on the flow of powell-eyring fluid past an unsteady inclined stretching sheet with non-uniform heat source/sink," *PLoS ONE*, vol. 9, no. 7, Article ID e103214, 2014.

[17] V. Sirohi, M. G. Timol, and N. L. Kalathia, "Numerical treatment of Powell-Eyring fluid flow past a 90 degree wedge," *Regional Journal of Energy, Heat and Mass Transfer*, vol. 6, no. 3, pp. 219–228, 1984.

[18] O. Adesanya and J. A. Gbadeyan, "Adomian decomposition approach to steady viscoelastic fluid flow with slip through a planar channel," *International Journal of Nonlinear Science*, vol. 9, pp. 86–94, 2010.

[19] V. R. Prasad, S. A. Gaffar, E. K. Reddy, and O. A. Bég, "Computational study of non-newtonian thermal convection from a vertical porous plate in a non-darcy porous medium with biot number effects," *Journal of Porous Media*, vol. 17, no. 7, pp. 601–622, 2014.

[20] L. Rosenhead, *Laminar Boundary Layers*, Oxford University Press, Oxford, UK, 1963.

[21] J. Peddieson, "Wedge and cone flows of viscoelastic liquids," *AIChE Journal*, vol. 19, no. 2, pp. 377–379, 1973.

[22] E. M. Sparrow, R. Eichhorn, and J. L. Gregg, "Combined forced and free convection in a boundary layer flow," *Physics of Fluids*, vol. 2, pp. 319–328, 1959.

[23] T. Watanabe, K. Funazaki, and H. Taniguchi, "Theoretical analysis on mixed convection boundary layer flow over a wedge with uniform suction or injection," *Acta Mechanica*, vol. 105, no. 1–4, pp. 133–141, 1994.

[24] N. G. Kafoussias and N. D. Nanousis, "Magnetohydrodynamic laminar boundary-layer flow over a wedge with suction or injection," *Canadian Journal of Physics*, vol. 75, no. 10, pp. 733–745, 1997.

[25] N. D. Nanousis, "Theoretical magnetohydrodynamic analysis of mixed convection boundary-layer flow over a wedge with uniform suction or injection," *Acta Mechanica*, vol. 138, no. 1-2, pp. 21–30, 1999.

[26] R. S. R. Gorla, "Unsteady heat transfer in laminar non-Newtonian boundary layer over a wedg," *AIChE Journal*, vol. 28, no. 1, pp. 56–60, 1982.

[27] K.-A. Yih, "Radiation effect on mixed convection over an isothermal wedge in porous media: the entire regime," *Heat Transfer Engineering*, vol. 22, no. 3, pp. 26–32, 2001.

[28] M. M. Rashidi, M. T. Rastegari, M. Asadi, and O. A. Bég, "A study of non-Newtonian flow and heat transfer over a non-isothermal wedge using the homotopy analysis method," *Chemical Engineering Communications*, vol. 199, no. 2, pp. 231–256, 2012.

[29] A. J. Chamkha, M. Mujtaba, A. Quadri, and C. Issa, "Thermal radiation effects on MHD forced convection flow adjacent to a non-isothermal wedge in the presence of a heat source or sink," *Heat and Mass Transfer*, vol. 39, no. 4, pp. 305–312, 2003.

[30] K.-L. Hsiao, "MHD mixed convection for viscoelastic fluid past a porous wedge," *International Journal of Non-Linear Mechanics*, vol. 46, no. 1, pp. 1–8, 2011.

[31] A. Ishak, R. Nazar, and I. Pop, "Moving wedge and flat plate in a micropolar fluid," *International Journal of Engineering Science*, vol. 44, no. 18-19, pp. 1225–1236, 2006.

[32] A. Ishak, R. Nazar, and I. Pop, "Moving wedge and flat plate in a power-law fluid," *International Journal of Non-Linear Mechanics*, vol. 46, no. 8, pp. 1017–1021, 2011.

[33] H. B. Keller, "Numerical methods in boundary-layer theory," *Annual Review of Fluid Mechanics*, vol. 10, pp. 417–433, 1978.

[34] O. Anwar Bég, "Numerical methods for multi-physical magnetohydrodynamics," in *New Developments in Hydrodynamics Research*, chapter 1, pp. 1–112, Nova Science, New York, NY, USA, 2012.

[35] Y. Y. Lok, I. Pop, and D. B. Ingham, "Oblique stagnation slip flow of a micropolar fluid," *Meccanica*, vol. 45, no. 2, pp. 187–198, 2010.

[36] T.-B. Chang, A. Mehmood, O. A. Bég, M. Narahari, M. N. Islam, and F. Ameen, "Numerical study of transient free convective mass transfer in a Walters-B viscoelastic flow with wall suction," *Communications in Nonlinear Science and Numerical Simulation*, vol. 16, no. 1, pp. 216–225, 2011.

[37] D. Srinivasacharya and K. Kaladhar, "Mixed convection flow of couple stress fluid in a non-Darcy porous medium with Soret and Dufour effects," *Journal of Applied Science and Engineering*, vol. 15, no. 4, pp. 415–422, 2012.

[38] S. A. Gaffar, V. R. Prasad, and O. A. Bég, "Computational analysis of magnetohydrodynamic free convection flow and heat transfer of non-Newtonian tangent hyperbolic fluid from a horizontal circular cylinder with partial slip," *International Journal of Applied and Computational Mathematics*, 2015.

[39] V. R. Prasad, S. A. Gaffar, and O. A. Bég, "Heat and mass transfer of nanofluid from horizontal cylinder to micropolar fluid," *Journal of Thermophysics and Heat Transfer*, vol. 29, no. 1, pp. 127–139, 2015.

[40] V. R. Prasad, S. A. Gaffar, E. K. Reddy, and O. A. Bég, "Numerical study of non-newtonian boundary layer flow of jeffreys fluid past a vertical porous plate in a non-darcy porous medium," *International Journal of Computational Methods in Engineering Science and Mechanics*, vol. 15, no. 4, pp. 372–389, 2014.

[41] R. M. Darji and M. G. Timol, "On invariance analysis of MHD boundary layer equations for non-Newtonian Williamson fluids," *International Journal of Advances in Applied Mathematics and Mechanics*, vol. 1, pp. 10–19, 2014.

[42] V. Singh and S. Agarwal, "Flow and heat transfer of Maxwell fluid with variable viscosity and thermal conductivity over an exponentially stretching sheet," *American Journal of Fluid Dynamics*, vol. 3, no. 4, pp. 87–95, 2013.

[43] S. Nakamura, *Applied Numerical Methods and Software*, Prentice-Hall, New York, NY, USA, 1995.

[44] O. A. Bég, T. A. Bég, H. S. Takhar, and A. Raptis, "Mathematical and numerical modeling of non-Newtonian thermo-hydrodynamic flow in non-Darcy porous media," *International Journal of Fluid Mechanics Research*, vol. 31, no. 1, pp. 1–12, 2004.

[45] I. Pop and S. Nakamura, "Laminar boundary layer flow of power-law fluids over wavy surfaces," *Acta Mechanica*, vol. 115, no. 1–4, pp. 55–65, 1996.

[46] R. S. R. Gorla, A. Slaouti, and H. S. Takhar, "Free convection in micropolar fluids over a uniformly heated vertical plate," *International Journal of Numerical Methods for Heat & Fluid Flow*, vol. 8, no. 5-6, pp. 504–518, 1998.

[47] O. A. Bég, V. R. Prasad, and B. Vasu, "Numerical study of mixed bioconvection in porous media saturated with nanofluid containing oxytactic microorganisms," *Journal of Mechanics in Medicine and Biology*, vol. 13, no. 4, Article ID 1350067, 2013.

[48] O. Anwar Bég, J. Zueco, M. Norouzi, M. Davoodi, A. A. Joneidi, and A. F. Elsayed, "Network and Nakamura tridiagonal computational simulation of electrically-conducting biopolymer micro-morphic transport phenomena," *Computers in Biology and Medicine*, vol. 44, no. 1, pp. 44–56, 2014.

[49] N. A. Yacob, A. Ishak, and I. Pop, "Falkner-Skan problem for a static or moving wedge in nanofluids," *International Journal of Thermal Sciences*, vol. 50, no. 2, pp. 133–139, 2011.